International Journal of Design & Nature and Ecodynamics
Vol. 21, No. 6, June, 2026, pp. 1625-1638
Journal homepage: http://iieta.org/journals/ijdne

Techno-Economic and Thermodynamic Evaluation of Low-Emission Hydrogen Production Pathways for Steel Decarbonization: A Peruvian Case Study

Diego Vera Sullayme, Jesús Ticona Quispe, Pascual Adriazola Corrales, José Villanueva Salazar, Christofer Alex Diaz Arapa*

Department of Mechanical Engineering, Universidad Nacional de San Agustín de Arequipa, Arequipa 04000, Perú

Corresponding Author Email: cdiazar@unsa.edu.pe

https://doi.org/10.18280/ijdne.210610

Received: 15 April 2026
Revised: 18 June 2026
Accepted: 25 June 2026
Available online: 30 June 2026

Keywords:
green hydrogen, blue hydrogen, proton exchange membrane electrolysis, autothermal reforming, levelized cost of hydrogen, decarbonization

ABSTRACT

The steel industry faced a critical challenge due to its significant contribution to global CO_2 emissions, mainly derived from the use of fossil fuels in conventional processes. This situation created an urgent need for more sustainable alternatives. Hydrogen emerged as a key energy carrier for decarbonization, particularly in its green and blue forms. These options demonstrated strong potential to reduce emissions through electrolysis powered by renewable energy sources and natural gas reforming with CO_2 capture, respectively. In this context, the present study aimed to comparatively evaluate the feasibility of implementing green and blue hydrogen for steel production in Peru from a techno-economic perspective. The methodology was based on Aspen Plus scenario simulations of proton exchange membrane (PEM) electrolysis and autothermal reforming (ATR) with methyldiethanolamine (MDEA)-based carbon capture, followed by a techno-economic assessment using the levelized cost of hydrogen (LCOH). The simulations showed that a continuous hydrogen production target of 0.16 kg/s required approximately 28.8 MW of PEM electrolyzer power. Green hydrogen production increased linearly with electrical input, while blue hydrogen performance depended strongly on ATR operating conditions. The estimated LCOH was 6.78 USD/kg for green hydrogen and 3.83 USD/kg for blue hydrogen, making the latter approximately 43% less expensive. The comparison focused on process-related CO_2 emissions rather than a full life-cycle carbon intensity assessment. This highlighted the trade-off between sustainability and economic feasibility.

1. INTRODUCTION

Industrial processes play a crucial role in the development of various sectors worldwide, but they are energy-intensive and, above all, emit excessive amounts of CO_2 [1]. Specifically, the steel industry is used in infrastructure, energy, mining, transportation, manufacturing, and other fields; steel production is one of the fundamental pillars of economic and industrial development worldwide [2]. The problem with this industry lies in the fact that it has a large carbon footprint compared to other types of industries [3]. Globally, the steel industry accounts for approximately 8% of greenhouse gas emissions and 11% of human-caused global carbon dioxide (GHG) emissions [4], particularly due to the use of energy sources such as natural gas and coal in various types of furnaces. In the current context, where a shift is needed in how we produce, consume, and live, given that climate change already threatens our very existence, the tightening of environmental regulatory frameworks and compliance with international treaties, the transformation of the steel industry toward a process with very low or zero carbon emissions has become essential for advancing toward more sustainable production models worldwide. Figure 1 shows the percentage of GHG emissions from various sectors, including a portion of the emissions from the electricity consumed by those sectors [5], and Figure 2 shows the percentage of emissions from the steel industry relative to other types of industries.

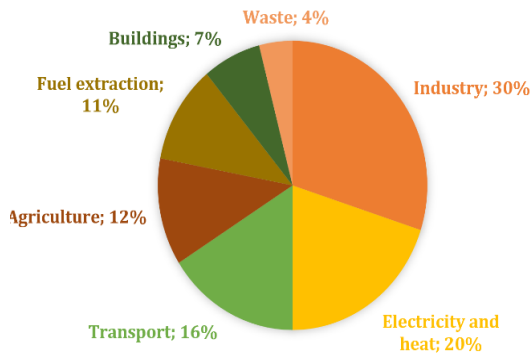

Figure 1. Greenhouse gas (GHG) emissions as a percentage caused by different sectors

As shown in the figure, the industrial sector accounts for the largest percentage of global GHG emissions. This sector is further divided into subsectors such as steel, cement, chemicals, and petrochemicals, among others; these

subsectors also contribute significantly to pollution through their processes. An important figure is the estimated global CO_2 emissions, which amount to 37 Gt CO_2/year [6]. This value is useful for estimating CO_2 emissions in the industrial subsectors, as shown in Figure 2.

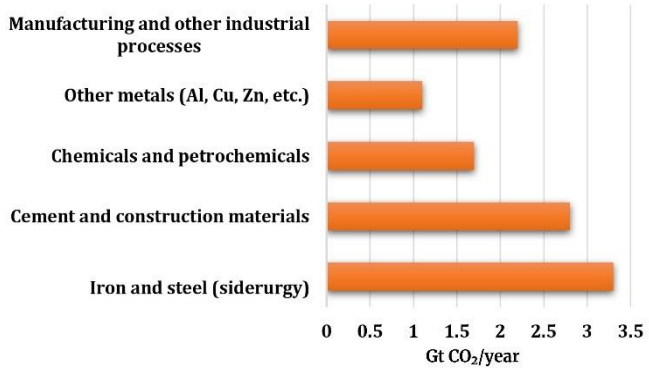

Figure 2. CO_2 emissions in Gt/year for each industrial sub-process [7]

In the context of the energy transition, a potential solution has emerged: the use of hydrogen as an energy carrier for the decarbonization of various industries, such as the steel industry. Using hydrogen as a reducing agent for iron ore allows for a significant reduction or complete elimination of CO_2 emissions in the process [8]. However, this hydrogen is categorized by various colors, such as green, blue, gray, pink, brown, etc., which are related to its production method and carbon emission levels; the resulting CO_2 emissions depend on these factors. Of these colors, green and blue hydrogen are of greater interest to the scientific community for industrial applications on a large scale, as they achieve a total or near 100% reduction in CO_2 emissions.

Blue hydrogen is produced through natural gas reforming, but to be classified as blue, it must be accompanied by a carbon capture system for subsequent use or storage; otherwise, it would be called gray hydrogen. This option allows for a significant reduction in carbon dioxide emissions as long as high capture rates are achieved; according to the study [9], it is demonstrated that blue hydrogen can be a powerful tool for the transition to a low-carbon economy and that it has significant room for improvement through the optimization of methods and infrastructure. Variations in conventional processes for producing blue hydrogen and capturing CO_2 can be found in the studies [10-13], where the optimization of blue hydrogen production and CO_2 capture is discussed.

On the other hand, green hydrogen is produced through the electrolysis of water using an electrolyzer, provided that the electrolyzer is powered by electricity generated from renewable sources such as solar or wind. This method of hydrogen production emits zero percent CO_2 since it contains no carbon in its chemical composition; however, this method currently entails high costs and a high demand for electricity [14]. In the study [15], the author presents a study on green and blue hydrogen, as well as the combination of both for the production of hydrogen and subsequently ammonia, highlighting that this combination is a promising solution for the future and can bring greater visibility to the potential of green hydrogen.

Despite the rapid growth of all these scientific studies, both theoretical and applied, on the use of various types of hydrogen for various industries, particularly the steel industry, there are technical and economic uncertainties. Specifically, there is a great need for further technical evaluations regarding system efficiency, investment, and operating costs; all of this combined with product storage, prices of raw materials such as natural gas, and economic penalties or incentives resulting from carbon policies. This study is presented within a Peruvian case context. The hydrogen demand was estimated based on the projected Direct Reduced Iron (DRI) requirements of the Peruvian steel industry, using publicly available information from Aceros Arequipa and national climate policies. However, the techno-economic parameters employed in the simulations, including electrolyzer performance, autothermal reforming (ATR) operation, and cost correlations, were primarily adopted from internationally validated literature to ensure methodological consistency and facilitate comparison with previous studies.

Several recent techno-economic studies have evaluated green hydrogen production through proton exchange membrane (PEM) electrolysis or blue hydrogen production using natural gas reforming with carbon capture. These studies have mainly focused on optimizing individual production pathways, evaluating hydrogen costs, or assessing environmental performance under generic operating conditions. However, direct comparisons between PEM electrolysis and ATR-methyldiethanolamine (MDEA) systems under a common industrial hydrogen demand scenario remain limited, particularly for applications related to steel decarbonization. To address this gap, this study performs a comparative thermodynamic and techno-economic assessment of green hydrogen (PEM electrolysis) and blue hydrogen (ATR with MDEA-based CO_2 capture) under a hydrogen demand representative of a Peruvian DRI steel production scenario. The comparison includes hydrogen production performance, process-related CO_2 emissions, and levelized cost of hydrogen (LCOH) using a consistent Aspen Plus simulation framework.

Consequently, this research aims to provide robust results and evidence that contribute to a transition toward a decarbonized steel industry through the use of hydrogen by identifying which type of hydrogen and which method is most suitable for the design of industrial strategies and future research focused on the decarbonization of various industrial sectors. Chapter 2 details the materials and methods used in the research, presenting the hydrogen production systems using blocks in the Aspen Plus software, covering both green hydrogen and blue hydrogen with carbon capture. Chapter 3 presents the research results, including technical and thermodynamic data, efficiencies, and a cost analysis, resulting in the cost of hydrogen over the plant's lifetime, all of which is based on simulations of the systems built in Aspen Plus; and Chapter 4 presents the results and recommendations for future research.

2. MATERIAL AND METHODS

This section describes the various methods, equations, and software employed to support the research findings. Proper implementation ensured the generation of accurate data aligned with the study objectives, which focused on reducing or eliminating global CO_2 emissions through hydrogen utilization. The research is based on ISO 14064, which helps companies manage their carbon footprint to improve their environmental performance, as well as Law 30754 and

Supreme Decree No. 012-2024-MINAM in Peru, which establishes the country's commitment to climate policies to fulfill Peru's obligations under the Paris Agreement [16, 17].

2.1 Steel industry

The steel industry is one of the cornerstones of many industrial sectors; its value chain spans from the sourcing of raw materials to the processes of steel reduction, melting, and refining, which involve various technologies such as blast furnaces and electric arc furnaces (EAF). The steel industry contributes a significant amount of pollution that cannot be ignored; as a result, it faces the challenge of decarbonizing its operations by adopting cleaner technologies.

In Peru, steel is widely used, particularly in construction, infrastructure, manufacturing, and mining. In this country, there are large companies such as Siderperu and Aceros Arequipa that are responsible for steel production; the latter has a structured plan to evaluate the use of green hydrogen starting in 2028. The progress made and next steps by Aceros Arequipa to support decarbonization are summarized in the timeline shown in Figure 3.

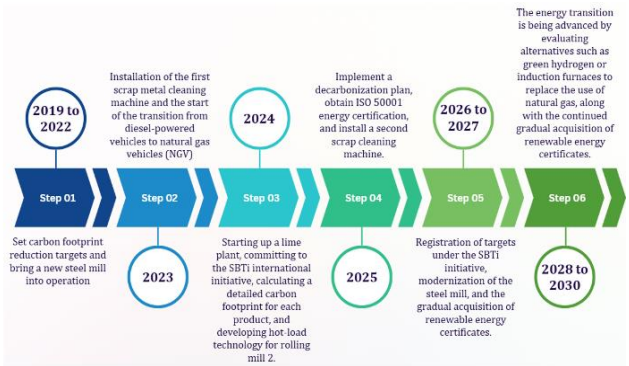

Figure 3. Timeline of progress made and steps to be taken for decarbonization according to Aceros Arequipa [18]

There are two main methods for producing steel. The first and most conventional method involves blast furnaces; this method is less costly and the most efficient, but it is highly polluting, as it generates approximately 2.3 tons of CO_2 per ton of steel [7, 19]. The second method involves EAF, which uses steel scrap or other materials that contain iron, such as DRI or heated briquetted iron (HBI), which is DRI that has been compacted [20]. These furnaces are less efficient and more expensive, but using them exclusively with scrap reduces CO_2 emissions by approximately 70% per ton of steel [7]. This research focuses on the DRI process using more eco-friendly alternative fuels and their production. DRI is iron obtained by reducing iron oxide with a reducing gas; this gas is obtained from natural gas reforming, but with a high percentage of hydrogen in the mixture or pure hydrogen, DRI is produced with very few or almost zero CO_2 emissions [21].

The use of DRI is necessary because a supply of good-quality scrap alone is not sufficient to meet the demand for steel; furthermore, adding DRI reduces impurities and produces higher-quality steel, which is essential for use in critical industries such as construction and mining [22, 23]. Steel production begins when iron ore is converted into DRI using hydrogen or natural gas, which removes oxygen from the ore; in the former, only H_2O is produced, and in the latter, CO_2. This DRI, along with scrap metal, is fed into the EAF to adjust the steel's composition and improve its quality. In the furnace, temperature and chemistry are controlled by injecting oxygen and adding alloying elements, resulting in molten steel that is then refined, solidified, and rolled into final products.

According to the study [24], at Aceros Arequipa, sponge iron, the product of the DRI process, is produced at the Pisco plant. This material represents approximately 30% of the metallic charge, while the remaining 70% consists of shredded recycled steel scrap. It is then poured into an electric furnace and heated to a temperature of 1600 °C; the molten steel is then transformed into steel billets, and finally undergoes the rolling process for subsequent sale.

The direct reduction reactor produces 90,000 metric tons of sponge iron per year [24]. In turn, approximately 50 to 60 kg of H_2 is required for every ton of DRI produced [25, 26]. Then, the required hydrogen production is approximately 5,046 metric tons per year (0.16 kg/s), which was used as the design basis for the simulations. The main operating parameters used to estimate the hydrogen demand are summarized in Table 1.

Table 1. Main operating parameters used to estimate hydrogen demand for the direct reduced iron (DRI) process

Parameters	Value
Continuous hydrogen production	0.16 kg/s
Annual H_2 required	5046 ton H_2/year
Hydrogen to produce DRI	55 kg H_2/tonn
Approximate energy consumption	45-55 KWh/kgH_2
Energy required at 0.16 kg/s and 50 kWh/kgH_2 in electrolyzer	28.8 MW
Higher Heating Value of Hydrogen	142 MJ/kg
Lower Heating Value of Hydrogen	120 MJ/kg

2.2 Green hydrogen production

Green hydrogen is seen as a solution for decarbonizing various industries that emit excessive amounts of CO_2, including the steel industry. By using water electrolysis powered by renewable energy, it produces a clean fuel that replaces the diesel, natural gas, or coal used in many sectors. This eliminates the main source of CO_2 emissions in steel manufacturing, paving the way toward a future of competitive and eco-friendly green steel [8]. This requires the integration of electrolyzers with wind or solar farms located in strategic areas to maximize the benefits of this method.

At the heart of this green technology is the electrolyzer, which contains an anode, a cathode, and an electrolyte; there are various types, such as the alkaline electrolyzer cell (AEC), the PEM electrolyzer, the solid oxide electrolyzer cell (SOEC), and the anion exchange membrane (AEM) electrolyzer; where the latter two are still under development, unlike the alkaline and PEM electrolyzers, whose technology is well-established; of these two, the PEM is more energy-efficient than the alkaline type by approximately 11% [27, 28].

The PEM electrolyzer uses a polymer membrane that separates water into hydrogen and oxygen by allowing protons to pass through while blocking electrons and gases. This is considered a superior method compared to others because it produces high-purity hydrogen, which is necessary for industrial applications, in addition to its high current density, energy efficiency, lower gas crossover, and better mass-volume ratio [29]. Many advantages are cited compared to

other hydrogen separation methods, but the main advantage lies in the fact that its performance is not affected by fluctuations in the power supply caused by the intermittent nature of wind and solar energy, all thanks to the rapid proton conduction of its membrane [30].

What allows protons to pass is the membrane electrode assembly; this system operates in an aqueous medium. The following are the equations for the water separation process using a PEM electrolyzer [31]:

$$H_2O \rightarrow \frac{1}{2}O_2 + 2H^+ + 2e^- \quad (1)$$

At the anode, the oxidation reaction occurs, where water molecules decompose, releasing oxygen, hydrogen ions (H^+), and electrons. This is shown in Eq. (1).

The protons, which are hydrogen ions, pass through the membrane electrode array, the electrons travel through an external circuit, and at the cathode, the reduction reaction takes place where the protons combine with the electrons to form hydrogen. This is shown in Eq. (2).

$$H^+ + 2e^- \rightarrow H_2 \quad (2)$$

The overall reaction corresponding to the electrolysis of water, which is considered an endothermic process driven by electrical energy, is presented in Eq. (3).

$$H_2 + \frac{1}{2}O_2 \rightarrow H_2O \quad (3)$$

To characterize the main parameters of the PEM system, equations are used to quantify energy performance; these are presented below, along with a brief introduction to each. To evaluate the electrolyzer performance, the energy efficiency was calculated as the ratio of the energy content of the produced hydrogen to the electrical energy supplied by renewable sources, as given in Eqs. (4)–(7) [30].

$$\eta PEM\ stack\ (LHV) = \frac{\dot{m}H_2 \times LHVH_2}{P_{Stack}} \quad (4)$$

$$\eta PEM\ stack\ (HHV) = \frac{\dot{m}H_2 \times HHVH_2}{P_{Stack}} \quad (5)$$

$$\eta PEM\ system\ (LHV) = \frac{\dot{m}H_2 \times LHVH_2}{P_{System}} \quad (6)$$

$$\eta PEM\ system\ (HHV) = \frac{\dot{m}H_2 \times HHVH_2}{P_{System}} \quad (7)$$

where,

$\dot{m}\ H_2$: hydrogen mass flow rate (kg/s)

$LHV\ H_2$: lower heating value of hydrogen (MJ/kg)

$HHV\ H_2$: higher heating value of hydrogen (MJ/kg)

P_{Stack}: power required by the PEM electrolyzer stack (MW)

P_{System}: Power required by the system (MW)

Faraday efficiency is also taken into account, which is very important for modeling the hydrogen and oxygen produced. The equation is presented below, where it is clarified that at low current densities, this efficiency is disproportionately low.

$$\eta_{Faraday} = \frac{Q_{ideal}}{Q_{real}} \quad (8)$$

where,

$\eta_{Faraday}$ = Faraday efficiency

Q_{ideal} = theoretical charge associated with the hydrogen generated according to Faraday's law (C)

Q_{real} = actual charge supplied to the electrolyzer during operation (C)

The voltage efficiency is now reported; this takes into account membrane and heat losses at the anode and cathode, and is typically lower than the Faraday efficiency because it considers only the losses caused by gas diffusion [32]. The following equations regarding voltage are taken from the study [33]. Energy is required to decompose water into its two components; this energy is necessary for the dissociation of water and is determined based on the change in Gibbs free energy (ΔG). This value represents the thermodynamic criterion that defines the essential energy threshold. It can be calculated with Eq. (9):

$$\Delta G = nFV_{rev} = \frac{237\ KJ}{mol} \quad (9)$$

where,

ΔG = Gibbs free energy

n = number of electrons involved (n = 2)

F = Faraday's constant = 96,500 C/mol

V_{rev} = Reversible voltage = 1.23 V [34]

On the other hand, in the dissociation of the water molecule, there is a change in entropy during the process; consequently, for estimating the thermodynamic potential, it is considered more appropriate to use the reaction enthalpy rather than Gibbs free energy. These data are necessary to determine the thermoneutral voltage, which is the minimum voltage required for the reaction to occur in the electrolytic cell; Eq. (10) represents this voltage.

$$V_{TN} = \frac{\Delta H}{nF} = \frac{\Delta G}{nF} + \frac{T\Delta S}{nF} = 1.4874V \quad (10)$$

where,

V_{TN} = Thermoneutral voltage

ΔG = Gibbs free energy

n = number of electrons involved (n = 2)

F = Faraday's constant = 96,500 C/mol

ΔH = Change in enthalpy = 285.574 kJ/mol-H_2O (according to the formula)

ΔS = Change in entropy = 0.163 kJ/mol K [32]

T = Ambient temperature (298 K)

Based on the first law of thermodynamics, energy is neither created nor destroyed, but only transformed. Accordingly, the conversion efficiency is calculated as the fraction of the supplied electrical energy that is converted into chemical energy. The voltage efficiency is given in Eq. (11).

$$\eta_{Voltage} = \frac{V_{TN}}{V_{cell}} \quad (11)$$

where,

$\eta_{Voltage}$ = Voltage efficiency

V_{TN} = Thermoneutral voltage

V_{cell} = Operating cell voltage

According to the study [32], the 3 efficiencies are related, and this is reflected in Eq. (12):

$$\eta_{Electrolyzer} = \eta_{Faraday} * \eta_{Voltage} \quad (12)$$

where,

$\eta_{Electrolyzer}$ = Electrolyzer efficiency

$\eta_{Faraday}$ = Faraday efficiency

$\eta_{Voltage}$ = Voltage efficiency

Unlike previous versions, version 14 of the Aspen Plus software implements an icon representing the electrolyzer and guides us, based on previous research, in the block modeling of a PEM electrolyzer with storage for later use [30, 34]. The PEM electrolyzer is represented in Figure 4.

The figure shows the introduction of deionized (H_2O) and ultrapure water for this purpose; it can be seen that this water is mixed with the water coming from the RECYCLE stream, which is recycled water from the liquid and gas separators (SEP1 and SEP2). Both the deionized and recycled water enter a pump (PUMP) operating at 36 bar; the feed water is preheated to 50 °C before entering the PEM electrolyzer. The electrochemical reactions inside the electrolyzer (PEMELECT) are carried out at an operating temperature of 70 °C, which was used as the operating condition in the Aspen Plus model, where various parameters, such as efficiencies and power, among others, that affect hydrogen production, can be set; this will be analyzed in the results section. In PEMELECT, the separation into H_2 and O_2 takes place. In the cell, neither in the anode nor in the cathode zones nor in the separators is any heat exchange considered to occur. To maintain pressure on each side, throttle valves are used to maintain 36 and 3.6 bar at the cathode and anode, respectively. Each stream contains a percentage of water, which is separated from the H_2 and O_2 in SEP1 and SEP2. From there, the water is recirculated to be combined with the feed stream, and the oxygen is directed to other industrial applications.

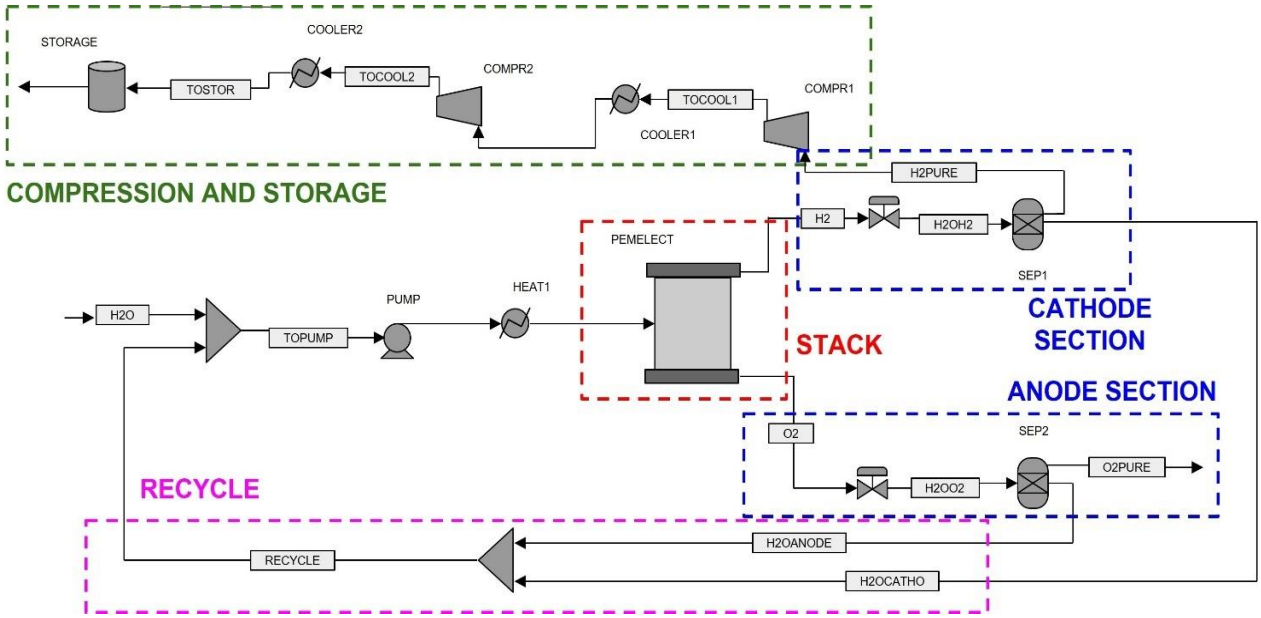

Figure 4. Green hydrogen production and storage using a proton exchange membrane (PEM) electrolyzer modeled in Aspen Plus

Table 2. Main parameters used in the proton exchange membrane (PEM) electrolyzer [30, 34-36]

Parameters	Value
Anode pressure	3.6 bar
Cathode pressure	36 bar
Purity of extracted H_2	99.99%
Operating temperature	70 °C
Water requirement needed for 1 kg of hydrogen	17.5 L/kg of H_2
Water requirement for 0.16 kg/s of H_2	2.8 kg/s
Oxygen Production	1.28 kg/s
Pump power	17 kW
Pump efficiency	0.75
Compressor power 1 and 2	260 and 267 kW
Isentropic efficiency of the compressor	90%
Mechanical efficiency of the compressor	99%
PEM electrolyzer cell efficiency (HHV)	78.89%
PEM electrolyzer cell efficiency (LHV)	66.67%
PEM electrolyzer system efficiency (HHV)	77.43%
PEM electrolyzer system efficiency (LHV)	65.43%
Faraday efficiency	99.99%
Voltage efficiency	79.45%

The hydrogen reaches a purity of 99.99% through other processes; it is then sent to the two-stage compression stage (COMPR1 and COMPR2) to compress the hydrogen from 36 to 200 bar, with intermediate cooling (COOLER 1 and COOLER 2), since compressing the hydrogen also raises its temperature, all of which ensures proper storage in a storage tank (STORAGE). Hydrogen storage was modeled without storage losses, assuming a storage efficiency of 100% [30]. In Aspen Plus, the PEM electrolyzer was modeled using an RStoic reactor operating at 70 °C. Gas-liquid separation was performed using flash blocks, hydrogen compression was modeled with compressor blocks assuming the specified isentropic efficiency, and hydrogen storage was represented by a storage vessel operating at the design pressure. The main parameters used in the PEM electrolyzer are presented in Table 2.

Renewable electricity was assumed to be supplied by a photovoltaic (PV) system with a representative capacity factor of 25%, consistent with the high solar resource available in southern Peru. To ensure continuous hydrogen production, the conceptual energy supply configuration includes a lithium-ion Battery Energy Storage System (BESS), intended to provide electricity during nighttime operation and to mitigate short-term fluctuations in PV generation. In addition, an emergency backup connection to the Peruvian National Interconnected Electric System (SEIN) was assumed through the regional transmission network, whose electricity mix is largely

supported by hydroelectric generation. Under these assumptions, the PEM electrolyzer was considered to operate continuously at a constant electrical input of 28.8 MW, maintaining the target hydrogen production rate of 0.16 kg/s throughout the simulations. The battery storage system and grid backup were introduced as operational assumptions to ensure an uninterrupted power supply and were not included in the techno-economic optimization or dynamic simulation of the renewable energy system.

2.3 Blue hydrogen production

To produce hydrogen, there are industrial processes such as steam methane reforming (SMR) and ATR. The latter is better for carbon capture and, therefore, the production of blue hydrogen, while SMR is more commonly used for the production of gray hydrogen [37].

ATR is an advanced technology for the production of synthesis gas (CO + H_2). This process does not require a significant heat input; the methane reacts with oxygen and steam, generating a highly efficient and compact system. Natural gas from Camisea will be used for this purpose, along with oxygen, both with compositions extracted from the studies [38, 39]. The compositions of Camisea natural gas and oxygen used in the simulations are summarized in Table 3.

Table 3. Composition of Camisea gas and oxygen

Element	Composition
Camisea Natural Gas	
Methane (CH_4)	88.54%
Ethane (C_2H_6)	10.32%
Propane (C_3H_8)	0.02%
Nitrogen (N_2)	0.54%
Carbon Dioxide (CO_2)	0.58%
Oxygen	
Oxygen (O_2)	95%
Argon (Ar)	3.4%
Nitrogen (N_2)	1.6%

Natural gas, which is primarily methane in an ATR, is converted into synthesis gas through a reaction between the natural gas, oxygen, and water vapor. This is followed by a process called the Water Gas Shift (WGS), in which carbon monoxide reacts with water vapor to produce more hydrogen and CO_2 for subsequent capture; this is an essential step for increasing hydrogen production and ensuring proper CO_2 capture. To better understand synthesis gas, the module number (M) is used, which is defined by Eq. (13).

$$M = \frac{H_2 - CO_2}{CO + CO_2} \tag{13}$$

To represent different efficiencies in the ATR, we present formulas that will serve this purpose. First, the reforming efficiency, which is based on the studies [40, 41], is modified since the objective of this work is to use only hydrogen and capture CO_2; CO, which also has a calorific value, should not be included here. Eq. (14) represents the usable chemical energy relative to natural gas:

$$\eta_{ATR} = \frac{\dot{m}H_2 \times LHVH_2}{\dot{m}NG \times LHVNG} \tag{14}$$

where, the mass flow rate is expressed in kg/s and the LHV in MJ/kg. In addition to this formula, we will also observe the conversion of carbon to gas and the hydrogen yield; the Eqs. (15) and (16) are taken from the study [42]:

$$H_2Yield = \frac{n_{H_2,prod}}{n_{H_2,NG} + n_{H_2,ATR} + n_{H_2,WGS}} \tag{15}$$

$$Carbon\ convertion = \frac{n_{C,product}}{n_{C,feed}} \tag{16}$$

Figure 5 illustrates the process described above. The implementation of this process in Aspen is based on the study [43].

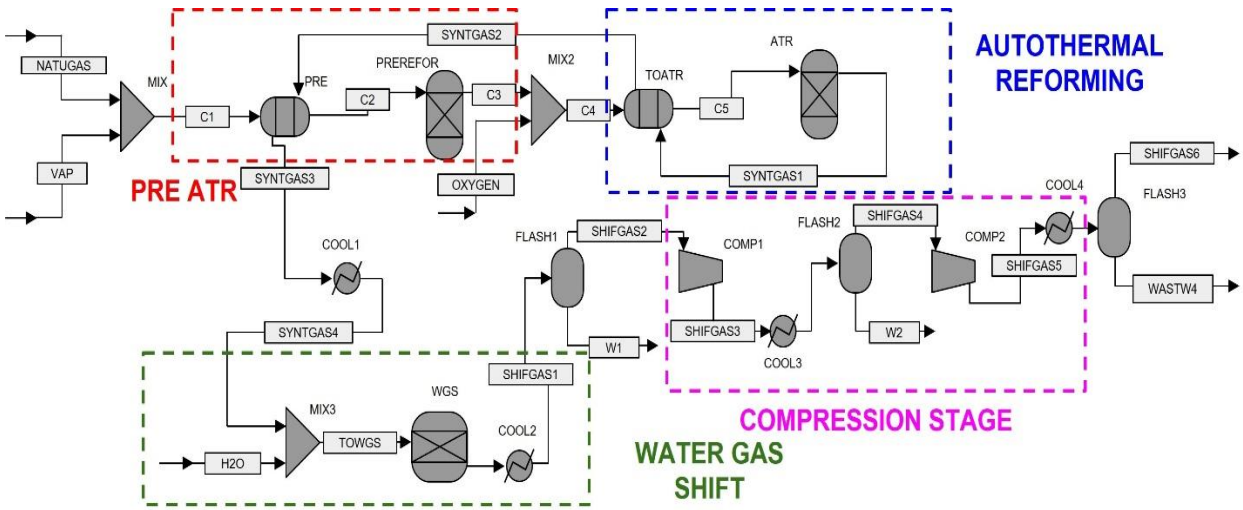

Figure 5. Hydrogen production using autothermal reforming (ATR) and water gas shift (WGS), followed by modeling in Aspen Plus

Firstly, natural gas is mixed with steam; in the first heat exchanger (PRE), it is heated to 500 °C, then enters the pre-reformer (PREREFOR), which operates adiabatically at 3 bar; here, almost all heavy hydrocarbons are converted into methane, CO, CO_2, and H_2. It is then mixed with 95% pure oxygen and enters another heat exchanger (TOATR) at 650 °C; this mixture enters the ATR reactor, where the methane is converted exothermically into syngas. Changes in

the temperatures of the two heat exchangers affect syngas production and the hydrogen percentage, always staying within the specified ranges to avoid damaging the equipment. The hot gas is used to preheat the feed stream, then cooled in (COOL1) to 25 °C; the synthetic gas is combined with steam (MIX3) to undergo the WGS process, then cooled to 25 °C in a cooler (COOL2). It then passes through isothermal flash drums (FLASH1, FLASH$_2$, and FLASH3) to separate the aqueous phase, as this could cause corrosion and problems in the subsequent compression unit. The synthesis gas in the intermediate stage passes through compressors (COMP1 and COMP2) with intermediate cooling (COOL3 and COOL4); compression is necessary to prepare it for the next step, which is carbon capture. The ATR, WGS, and CO_2 capture models were implemented in Aspen Plus following the operating conditions and process configurations reported in the referenced studies [43-47]. The simulations were developed under steady-state conditions, and the operating temperatures, pressures, flow rates, and unit specifications adopted for each process are summarized in Tables 4 and 5. The main process streams and operating conditions were selected to reproduce a hydrogen production rate of 0.16 kg/s for comparison with the PEM route. Table 4 shows the parameters used in the ATR.

Table 4. Main parameters of the autothermal reforming (ATR) [43, 44]

Parameters	Value
Pre - reforming pressure	3 bar
Pre - reforming temperature	500 °C
Natural gas flow	0.45 kg/s
Water vapor flow	0.6 kg/s
Water to WGS	0.5 kg/s
Temperature of WGS	200 °C
H_2O/CH_4 (kmol/kmol)	1.48
ATR Temperature	650 °C
Oxygen flow	0.48 kg/s
O_2/CH_4 (kmol/kmol)	0.63
M	1.86
H_2	0.16 kg/s
Dry syngas produced	1.42 kg/s
CO_2 produced	98.391 kmol/h
CH_4 conversion	99.95%
Compression stages	2
Pressure ratio of compressor	3:1
Isentropic efficiency of the compressor	80%
Mechanical efficiency of the compressor	99%
Power of the two compressors	901.749 kW
Cooling between stages	45 °C
Lower Heating Value of Camisea Gas	50 MJ/kg
Calorific Value of Carbon Monoxide	10.1 MJ/kg
ATR Efficiency without WGS	62.6%
ATR Efficiency with WGS	85.4%

For gray hydrogen to become blue hydrogen, a key technology for reducing carbon emissions is required: the capture of carbon dioxide for future applications. For this reason, capture using amine solutions is one of the most widely used technologies. In this research, MDEA is used because it has a high capture efficiency exceeding 90% as well as lower energy consumption [45]. Figure 6 shows the model in Aspen Plus using a RadFrac block and referencing [46]. The CO_2 capture efficiency was determined from the simulated CO_2 flow rates entering and leaving the absorption system, according to the mass balance of the capture process.

The solution is fed with syngas from the ATR, so that a hydrogen-enriched stream is produced and the MDEA can be recycled to continue the process. The simulation uses a composition of 30% MDEA and 70% H_2O in the stream (MDEA + H_2O). The parameters used in the simulation are listed in Table 5; some parameters are based on the research [47].

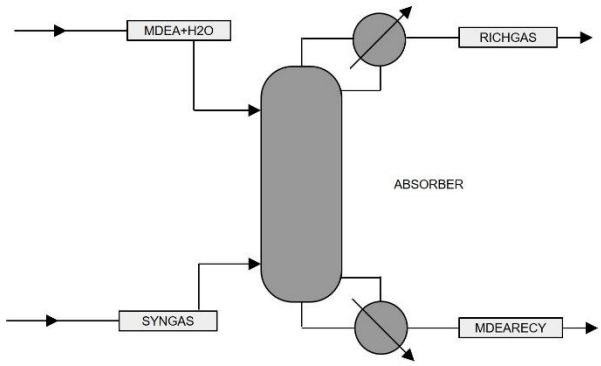

Figure 6. Carbon capture with methyldiethanolamine (MDEA) in Aspen Plus

Table 5. Main parameters of carbon capture

Parameters	Value
Pressure of the MDEA + H_2O solution	27 bar
Temperature of the MDEA + H_2O solution	24 °C
MDEA Flow	12.775 kg/s
Syngas temperature	45 °C
Syngas pressure	27 bar
Number of stages of the absorber	20

Table 6 shows the syngas composition after ATR that will be required for the simulation, with the parameters given in Table 4.

Table 6. Syngas composition

Element	Composition
Argon (Ar)	0.467%
Nitrogen (N_2)	0.346%
Hydrogen (H_2)	73.174%
Water Vapour (H_2O)	0.323%
Carbon Monoxide (CO)	0.5%
Carbon dioxide (CO_2)	25.18%
Methane (CH_4)	0.01%

3. RESULTS AND DISCUSSIONS

This section presents the results obtained from simulations conducted in Aspen Plus, varying different parameters such as efficiencies, temperatures, and energy requirements, among others, to observe the changes that occur in the production of green or blue hydrogen, CO_2 separation, CO_2 reduction, and various other parameters discussed in this section. The goal is to identify the most favorable alternative for steelmaking applications and contribute to a low-carbon industrial transition.

3.1 Results of simulation in Aspen Plus

First, we will examine how the supplied power affects green hydrogen production, as shown in Figure 7.

A linear and proportional relationship can be observed in both graphs; this follows the electrochemical kinetics of

Faraday's Law for electrolysis, which states that the amount of substance released is proportional to the electrical charge supplied to the electrolytic cell. In the case of Figure 7(a), an increase in mass flow of approximately 250% is observed from 8 MW to 28.8 MW, which is supplied in this experiment. Similarly, Figure 7(b) shows the behavior of the generated oxygen, which exhibits a similar growth trend throughout the graph, with an approximate 500% increase in mass flow from peak to peak, demonstrating thermodynamic consistency and validating the reliability of the system used. Figure 8 illustrates the role of efficiency in hydrogen production.

This graph helps us understand how electrochemical performance determines green hydrogen production for steelmaking applications. HHV, LHV, and voltage efficiencies represent three approaches that complement the previous figure, illustrating the conversion of electrical energy into chemical energy. First, regarding HHV efficiency, from the lowest value up to the operating efficiency of 0.16 kg/s, there is an approximate 28% increase in production; the specified steelmaking requirement of 0.16 kg/s is achieved at around 80% HHV, implying that the system must operate in a high-efficiency region to sustain the continuous demand of the direct iron reduction process. In the case of LHV, which is widely used in industrial evaluations because it excludes the latent heat of water vapor, there is an increase in hydrogen flow from 0.1561 kg/s to 0.1886 kg/s when efficiency increases from 65% to 79%, equivalent to a 20.8% increase. It should be noted that an LHV efficiency of approximately 68% is required to reach the target of 0.16 kg/s. Finally, by increasing the voltage efficiency from 76% to 90%, hydrogen production rises from 0.1536 kg/s to 0.1808 kg/s, representing a 17.7% increase. The required rate of 0.16 kg/s is achieved at around 80%, where the electrolyzer operates with minimal overpotential and the response becomes nearly linear, allowing for precise control through small electrical adjustments.

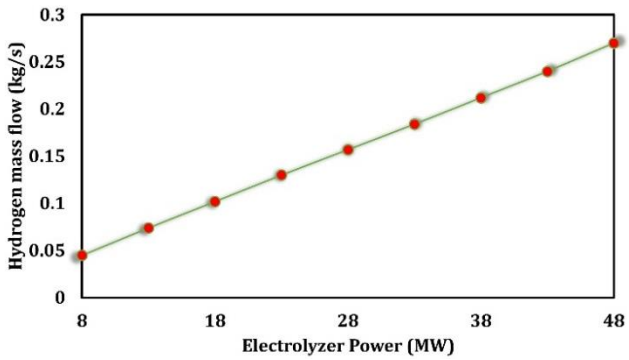

(a)

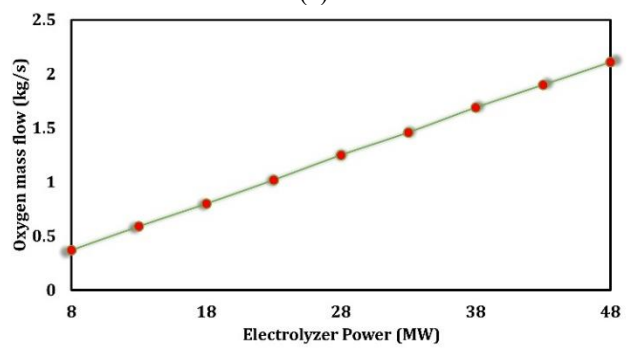

(b)

Figure 7. (a) Hydrogen mass flow and (b) oxygen mass flow as a function of the power supplied to the electrolyzer

The analysis shows that it is not recommended to operate the electrolyzer at its absolute minimum production limit. An additional margin of 3 to 6% ensures greater stability against electrical fluctuations, membrane degradation, and variations in demand at the DRI reactor. Therefore, the choice of operating point must balance energy efficiency, stability, and sustainability, thereby establishing a design criterion compatible with the sustainable production of green hydrogen for the steel industry.

We now analyze changes in various parameters in the ATR to see how they affect the results, both in terms of efficiency and hydrogen yield. Figure 9 shows the change in the Module Number "M" as the presented ratios are altered.

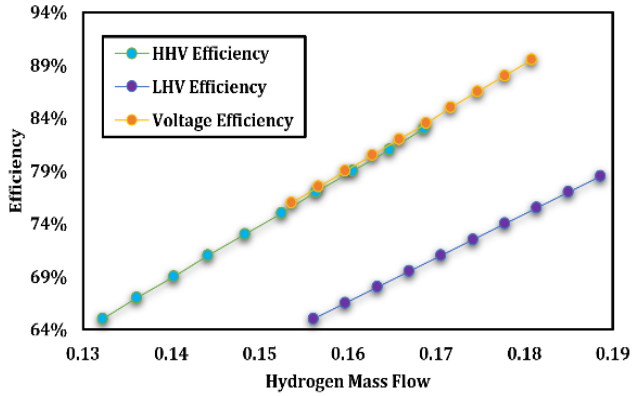

Figure 8. The role of different efficiencies in green hydrogen production

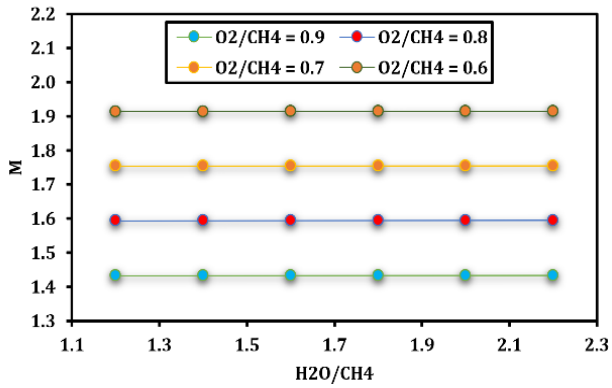

Figure 9. Effect of the O_2/CH_4 and H_2O/CH_4 ratios on the M modulus

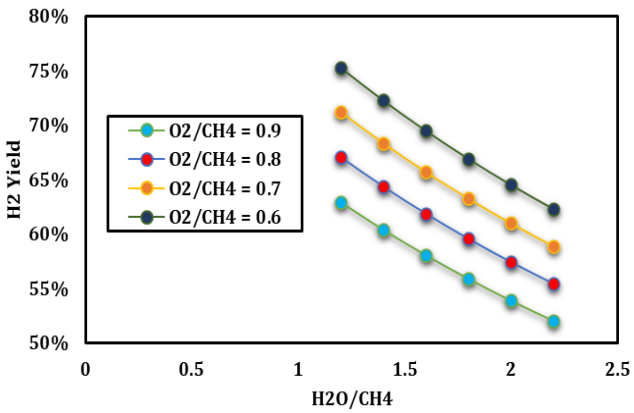

Figure 10. Effect of the O_2/CH_4 and H_2O/CH_4 ratios on H_2 yield

The figure shows that changing the H_2O/CH_4 ratio produces almost imperceptible variations in the value of M. In contrast, changes in the O_2/CH_4 ratio do result in significant changes, approximately a 25% change from one extreme to the other, which reflects that the increase in oxygen favors methane oxidation reactions, altering the composition of the synthesis gas and reducing the value of the M-modulus. All of this is consistent with the research [43], except that in our study, the analysis was performed after WGS. Figure 10 analyzes the H_2 yield by modifying the same ratios.

The figure shows the variation in hydrogen yield as a function of the H_2O/CH_4 ratio for different O_2/CH_4 ratios in the ATR. It can be seen that, for all operating conditions, the hydrogen yield decreases by approximately 31% as the H_2O/CH_4 ratio increases, since an excess of steam can dilute the reactive mixture, reducing the partial concentrations of methane and the products formed. In the case of the O_2/CH_4 ratio (0.6 to 0.9), it decreases by approximately 16% because a higher amount of oxygen favors partial oxidation reactions of methane, where part of the hydrogen formed is consumed to produce H_2O and CO_2, thereby lowering the hydrogen yield. For these reasons, in industrial ATR processes, an optimal balance between CH_4, H_2O, and O_2 is sought, since an excess of steam does not necessarily increase hydrogen production and may even decrease process efficiency. Figure 11 shows the results of hydrogen mass flow and ATR efficiency with respect to changes in the O_2/CH_4 ratio.

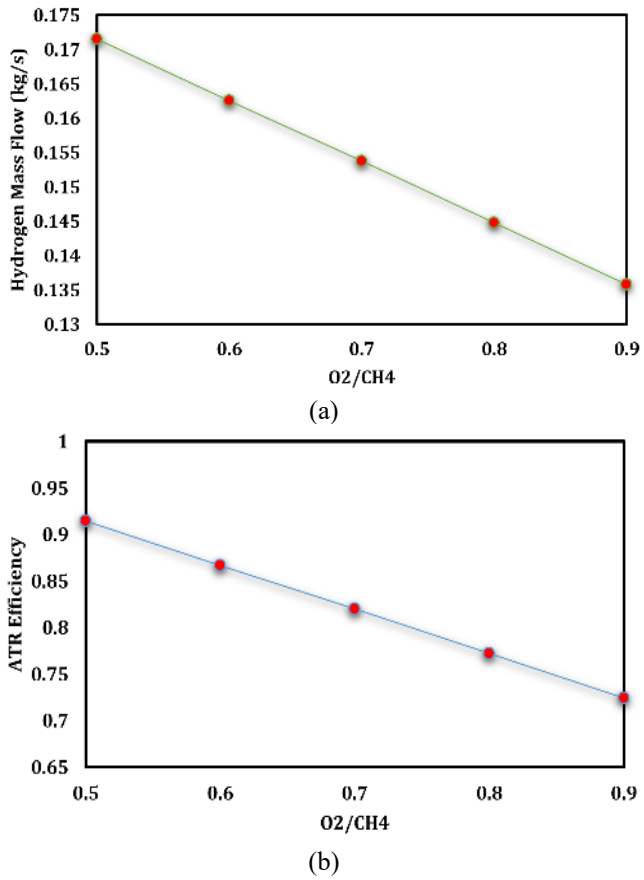

Figure 11. Effect of the O_2/CH_4 ratio on (a) the resulting hydrogen mass flow and (b) autothermal reforming (ATR) efficiency

It can be observed in Figure 11(a) that as the O_2/CH_4 ratio increases from 0.5 to 0.9, the hydrogen mass flow rate decreases progressively by approximately 20%, with the same explanation as for hydrogen yield. In Figure 11(b), it is shown that the ATR efficiency also decreases as the studied ratio increases. All of this demonstrates that although oxygen is necessary to maintain the reactor's thermal balance, an excess can reduce both hydrogen production and system efficiency. Therefore, it is important to operate within an optimal range of the O_2/CH_4 ratio to maximize process yield. Figure 12 shows how the natural gas mass flow rate affects the hydrogen and CO_2 mass flow rates.

Figure 12(a) shows that as the natural gas flow increases, the resulting hydrogen flow also increases by approximately 116% between the extremes, since there is a greater amount of methane available for increased synthesis gas production. However, at higher values on the curve, the slope begins to decrease because hydrogen is no longer proportional to methane, as the equipment and reactor begin to approach their limits. In Figure 12(b), it is observed that the increase in emissions from one extreme to the other is approximately 75%; this is because a greater amount of methane fed into the system generates more carbon available for oxidation during the process reactions. As shown in Figure 12(a), the curve shows a decrease in the final section for the same reason of limitations when injecting more natural gas into the equipment.

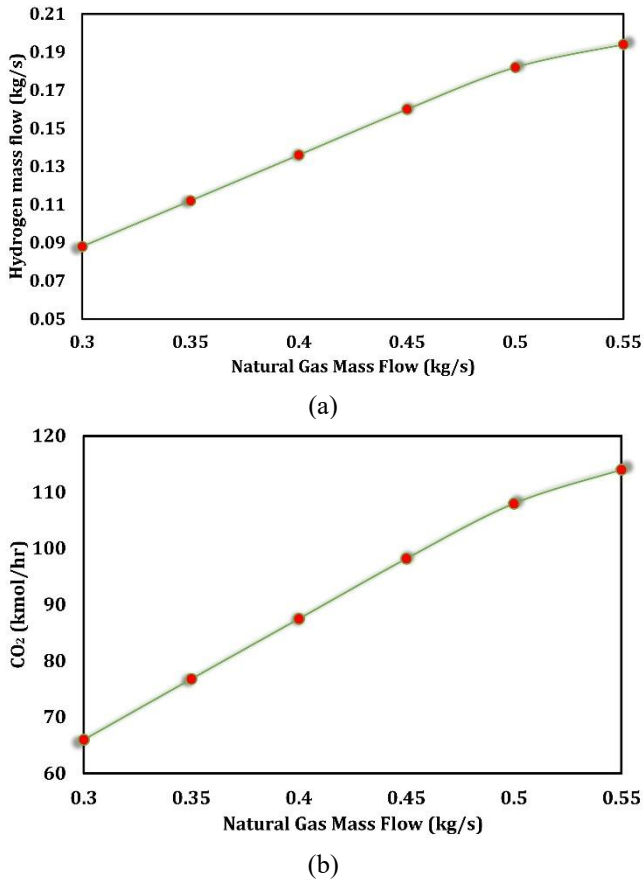

Figure 12. Effect of changes in natural gas on (a) hydrogen mass flow and (b) CO_2 emissions

We now analyze the CO_2 emissions of the different types of hydrogen examined in this study. It is important to note that we quantify the CO_2 from the process itself, not from indirect emissions such as solar panels, infrastructure, etc. It should be noted that green hydrogen, when accounting for indirect emissions and its entire life cycle, has an approximate value of 1 $kgCO_2/kgH_2$ [48]. With this clarified, Figure 13 shows the

emissions from the process of producing different types of hydrogen.

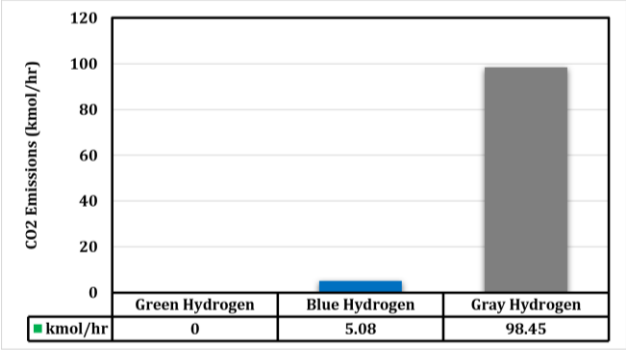

Figure 13. Recorded emissions of the different colors of hydrogen applied to this research

3.2 Cost analysis

This section of the research presents a cost analysis to compare the economic differences between the various types of hydrogen, as this is a crucial factor in selecting hydrogen production technology. The LCOH will be used for this analysis, as it is a key indicator that summarizes the total cost of producing one kilogram of hydrogen over the plant's lifetime. This research utilizes formulas from the study [49], primarily in Eq. (17) for the LCOH:

$$LCOH = \frac{\sum_{t=1}^{N} \frac{C_t + O_t}{(1+r)^t}}{\sum_{t=1}^{N} \frac{H_{2,t}}{(1+r)^t}} \quad (17)$$

where, C_t is the capital expenditure (CAPEX) incurred in year t (USD), O_t is the operating expenditure (OPEX) incurred in year t (USD/year), $H_{2,t}$ is the hydrogen produced in year t (kg/year), N is the project lifetime, assumed to be 28 years including a 3-year construction period, during which the CAPEX is distributed as 20%, 45%, and 35% over the first, second, and third years, respectively; r is the discount rate (8%), and t denotes the year [49].

We also need to determine the area covered by the PV panels for the implementation of green hydrogen, for which we use the formula from the study [50], presented in Eq. (18):

$$P_{PV} = \eta_{PV} \times A_{PV} \times G_{PV} \quad (18)$$

where, P_{PV} is the power generated by the photovoltaic system (W), η_{PV} is the photovoltaic conversion efficiency (20%), A_{PV} is the total photovoltaic panel area (m²), and G_{PV} is the incident solar irradiance (1,000 W/m²). In this study, the required photovoltaic power was assumed to be 29,000,000 W. Accordingly, the capital and operating costs associated with the BESS and the emergency grid connection were excluded from the LCOH calculation, as their role was limited to defining the operational boundary conditions of the process simulation rather than evaluating the complete energy infrastructure.

The CAPEX for the blue hydrogen production process is expressed in Eq. (19), as reported by the study [49], where each term represents the investment cost of the ATR and CO_2 capture system:

$$CAPEX(\$M) = 34.2 \times s^{0.414} \quad (19)$$

where, s is hydrogen produced in tons per day. To calculate the values needed to determine the LCOH, correlations taken from the studies [49, 51] were used and adapted to this project; all of this is shown in Table 7. The techno-economic assessment was performed using representative cost assumptions consistent with the Peruvian energy context and values commonly reported in the recent hydrogen literature. Electricity supplied from the PV system was assumed to have a levelized cost of 45 USD/MWh (0.045 USD/kWh). Natural gas was valued at 4.5 USD/MMBtu, representative of industrial supply from the Camisea gas network. Industrial water was assumed to cost 1.0 USD/m³, while oxygen produced as a by-product of PEM electrolysis was considered to have no economic credit because its commercialization was outside the scope of this study. Likewise, CO_2 transport and geological storage costs were not included in the economic assessment, since the analysis focused on the hydrogen production process and carbon capture stage rather than the complete CO_2 management chain. These assumptions were applied consistently to the LCOH calculations for both hydrogen production pathways.

Once all of this has been accounted for in the case of blue hydrogen, the LCOH increases by approximately $0.6/kg, as it also incorporates various stages such as flow compression and storage, and even the natural gas itself [49]. In the case of green hydrogen, all these stages are already included in the LCOH calculation; therefore, Table 8 shows the results of the approximate costs incurred in the experiment.

Table 7. Values and correlations used to calculate the levelized cost of hydrogen (LCOH)

Parameters	Value
Green Hydrogen	
Electrolyzer PEM CAPEX rate	$2,077/kW
Electrolyzer PEM CAPEX	$59,817,600
Electrolyzer PEM OPEX correlation	5% × Electrolyzer CAPEX rate
Electrolyzer PEM OPEX	OPEX Rate × Power (kW)
PV CAPEX rate	$540/m²
PV CAPEX	$ 78,300,000
PV OPEX correlation	5% × PV CAPEX
Blue Hydrogen (ATR + Carbon Capture)	
s	13.824 tons/day
CAPEX	101.45 M$
OPEX correlation	6% × CAPEX
OPEX	6.09 M$/year

Notes: PEM: Proton exchange membrane, CAPEX: Capital expenditure.

Table 8. Summary of costs for green and blue hydrogen

Technology	LCOH
Green Hydrogen	6.78 $/kg
Blue Hydrogen	3.83 $/kg

Notes: LCOH: Levelized cost of hydrogen.

The LCOH reflects how competitive each hydrogen production technology is; it shows that blue hydrogen is cheaper to produce than green hydrogen, given that technologies such as PEM electrolyzers and solar panels currently require significant investment as well as large tracts of land if solar energy is used. These results are consistent with research such as the study [49]. Despite its high cost, green hydrogen represents the most sustainable option with the

greatest future potential, as the technologies underpinning this method are becoming increasingly affordable. It is projected that costs could decrease by approximately 30% by 2030, thanks to more sophisticated technologies and reduced costs in renewable energy, all in the interest of protecting the planet's environment [52].

To further evaluate the influence of future decarbonization policies on the economic competitiveness of hydrogen production pathways, an additional carbon price sensitivity analysis was performed. Carbon pricing was applied only to the residual direct CO_2 emissions associated with the blue hydrogen production process (5.08 kmol/h), while green hydrogen was assumed to have no direct process-related CO_2 emissions. The analysis considered carbon prices ranging from 0 to 200 USD/tCO_2, covering representative values reported in international carbon market scenarios and long-term climate policy projections. The resulting effect on the LCOH is presented in Table 9.

As shown in Table 9, increasing carbon prices progressively increase the LCOH of blue hydrogen because of the additional cost associated with its residual CO_2 emissions. However, owing to the high CO_2 capture efficiency achieved in the MDEA absorption process, the increase in production cost remains relatively small, reaching only 3.91 USD/kg at a carbon price of 200 USD/tCO_2, which represents an increase of approximately 2.0% compared with the base case. In contrast, the LCOH of green hydrogen remains unchanged because the PEM electrolysis process does not generate direct process-related CO_2 emissions. These results indicate that carbon pricing alone is insufficient to eliminate the current economic advantage of blue hydrogen under the assumptions adopted in this study. Nevertheless, future reductions in renewable electricity costs, improvements in electrolyzer technology, and more stringent climate policies are expected to further enhance the long-term competitiveness of green hydrogen for steel decarbonization.

Table 9. Values and correlations used to calculate the levelized cost of hydrogen (LCOH)

Carbon Price (USD/tCO_2)	Green Hydrogen LCOH (USD/kg)	Blue Hydrogen LCOH (USD/kg)	Increase in Blue H_2 LCOH (%)
0	6.78	3.83	0.00
25	6.78	3.84	0.25
50	6.78	3.85	0.51
100	6.78	3.87	1.01
150	6.78	3.89	1.52
200	6.78	3.91	2.03

4. CONCLUSION

This study presents a simulation-based comparative assessment of green and blue hydrogen production pathways for steel decarbonization under a representative Peruvian case scenario. Green hydrogen, produced in this study using a PEM electrolyzer, exhibits a linear relationship between power and hydrogen production; within a range of 8 to 28.8 MW, it achieves an increase in hydrogen and oxygen of approximately 250% and 500%, respectively, validating the electrochemical consistency of the system; furthermore, it is necessary to operate at around 80% HHV efficiency to achieve the required 0.16 kg/s; additionally, a 28%, 20.8%, and 17.7% increase in production is observed when HHV, LHV, and voltage efficiencies are increased, respectively. On the other hand, blue hydrogen produced via ATR shows high sensitivity to operating parameters: increasing the O_2/CH_4 ratio reduces hydrogen yield by approximately 16% and its overall efficiency, while increasing the H_2O/CH_4 ratio can decrease it by up to 31%. Similarly, increasing the natural gas flow rate boosts hydrogen production by approximately 116%, but increases CO_2 emissions by around 75%, illustrating a trade-off between productivity and sustainability. Despite a CO_2 capture efficiency of over 90% in the MDEA carbon capture process, residual emissions still occur during blue hydrogen production; however, these are minimal compared to those of gray hydrogen. The LCOH cost analysis shows that the cost is \$3.83/kg, approximately 43% lower than that of green hydrogen, which is \$6.78/kg. Therefore, in the short term, it is the most competitive alternative. However, green hydrogen stands out for its potential for complete decarbonization and long-term sustainability, as this technology shows a strong trend toward lowering its implementation costs each year. Consequently, it is concluded that the choice of technology must balance costs, efficiency, and emissions reduction, with blue hydrogen standing out for its current economic viability, while green hydrogen offers the best long-term environmental alternative. It is recommended that the results obtained in this study be considered for future implementation in real industrial environments, in order to validate their performance under actual operating conditions and strengthen the reliability of the conclusions. Under this approach, decision-making in the Peruvian steel industry should focus on maximizing operational efficiency and reducing environmental impact, prioritizing optimized technological configurations that enable compliance with decarbonization goals without compromising economic viability. This study represents a simulation-based assessment developed under a Peruvian case context, while using internationally reported techno-economic parameters to enable broader comparison and reproducibility. Additionally, the costs and data used were mainly obtained from global sources, complemented with reference information from Aceros Arequipa as a guideline for the local context, in order to strengthen the representativeness of the study without limiting the assessment of technological and economic feasibility to a single region, thereby enabling more generalizable, comparable, and applicable results across different contexts with similar energy conditions, yielding consistent and satisfactory results.

The present study is intended as a preliminary simulation-based comparison and does not include dynamic renewable power fluctuations, hydrogen storage and transport, direct coupling with a DRI reactor, or industrial-scale validation. These aspects should be addressed in future work to support large-scale implementation.

REFERENCES

[1] Hu, Y., Man, Y. (2023). Energy consumption and carbon emissions forecasting for industrial processes: Status, challenges and perspectives. Renewable and Sustainable Energy Reviews, 182: 113405. https://doi.org/10.1016/J.RSER.2023.113405

[2] Bucur, A., Dobrotă, G., Oprean-Stan, C., Tănăsescu, C. (2017). Economic and qualitative determinants of the world steel production. Metals, 7(5): 163.

https://doi.org/10.3390/met7050163
[3] Zhang, X., Jiao, K., Zhang, J., Guo, Z. (2021). A review on low carbon emissions projects of steel industry in the World. Journal of Cleaner Production, 306: 127259. https://doi.org/10.1016/J.JCLEPRO.2021.127259
[4] Davis, C., Li, Z., Styring, P., Curry, R., Holliman, P.J. (2025). Routes to reducing emissions from steel production. Nature Reviews Clean Technology, 1(12): 890-902. https://doi.org/10.1038/s44359-025-00118-1
[5] Crippa, M., Guizzardi, D., Pagani, F., et al. (2024). GHG emissions of all world countries. Publications Office of the European Union. https://doi.org/10.2760/0115360
[6] Friedlingstein, P., O'Sullivan, M., Jones, M.W., et al. (2025). Global Carbon Budget 2024. Earth System Science Data, 17(3): 965-1039. https://doi.org/10.5194/essd-17-965-2025
[7] OECD. (2025). OECD Steel Outlook 2025. OECD Publishing. https://doi.org/10.1787/28b61a5e-en
[8] Bhaskar, A., Assadi, M., Somehsaraei, H.N. (2020). Decarbonization of the iron and steel industry with direct reduction of iron ore with green hydrogen. Energies, 13(3): 758. https://doi.org/10.3390/en13030758
[9] Tabrizi, M.K., Vitasari, C.R., Bonalumi, D., Campanari, S. (2026). Blue hydrogen can be low-carbon, a techno-economic-environmental analysis. Energy Conversion and Management, 348: 120608. https://doi.org/10.1016/J.ENCONMAN.2025.120608
[10] Yun, J., Ryu, K.H., Gu, B. (2025). Towards sustainable blue hydrogen: Integrating membrane-based carbon capture and oxygen-enriched combustion. Chemical Engineering Journal, 525: 169850. https://doi.org/10.1016/J.CEJ.2025.169850
[11] Li, Y., Ren, J., Ma, H., Campbell, A.N. (2024). Technical and economic performance assessment of blue hydrogen production using new configuration through modelling and simulation. International Journal of Greenhouse Gas Control, 134: 104112. https://doi.org/10.1016/J.IJGGC.2024.104112
[12] Yan, Y., Thanganadar, D., Clough, P.T., et al. (2020). Process simulations of blue hydrogen production by upgraded sorption enhanced steam methane reforming (SE-SMR) processes. Energy Conversion and Management, 222: 113144. https://doi.org/10.1016/J.ENCONMAN.2020.113144
[13] Ayub, Y., Zhou, J., Shi, T., Toniolo, S., Ren, J. (2025). Sustainability assessment of blue hydrogen production through biomass gasification: A comparative analysis of thermal, solar, and wind energy sources. Bioresource Technology, 418: 131798. https://doi.org/10.1016/J.BIORTECH.2024.131798
[14] Lin, K., Chen, B., Liu, Z., et al. (2025). Toward efficient, low-carbon, and Cost-effective hydrogen production shifting from fossil fuel-based to renewable water electrolysis: A perspective and outlook. Applied Energy, 401: 126661. https://doi.org/10.1016/J.APENERGY.2025.126661
[15] Biswas, S., Menon, A., Field, R., Zang, G., Green, W.H. (2025). A comprehensive costing and emissions analysis of blue, green, and combined blue-green ammonia production. Energy & Fuels, 39(38): 18694-18710. https://doi.org/10.1021/acs.energyfuels.5c03111
[16] Ministry of the Environment - MINAM. (2024). Supreme Decree No. 012-2024-MINAM: National Policy – National Strategy on Climate Change to 2050. 012-2024-MINAM. https://sinia.minam.gob.pe/normas/decreto-supremo-que-aprueba-politica-nacional-estrategia-nacional-ante.
[17] Ministry of the Environment of Peru. (2018). Law No. 30754: Framework Law on Climate Change. https://sinia.minam.gob.pe/normas/ley-marco-cambio-climatico.
[18] Corporación Aceros Arequipa. https://investors.acerosarequipa.com/memoria-integrada-2024/en/.
[19] Jiang, B., Tian, Z., Wang, Q., Xia, D., Wang, Y., Zhang, K. (2025). CO2 cut-down potential of conventional iron and steel making process in China based on carbon transfer and emission identification. Science of The Total Environment, 999: 180372. https://doi.org/10.1016/J.SCITOTENV.2025.180372
[20] Visuri, V.V., Echterhof, T. (2025). Electric Arc Furnace Steelmaking. Metals, 15(12): 1285. https://doi.org/10.3390/met15121285
[21] Ji, Y., Chi, Z., Yuan, S., et al. (2024). Development and application of hydrogen-based direct reduction iron process. Processes, 12(9): 1829. https://doi.org/10.3390/pr12091829
[22] Zakeri, A., Coley, K.S., Tafaghodi, L. (2023). Hydrogen-Based Direct Reduction of Iron Oxides: A Review on the Influence of Impurities. Sustainability, 15(17). https://doi.org/10.3390/su151713047
[23] Kirschen, M., Badr, K., Pfeifer, H. (2011). Influence of direct reduced iron on the energy balance of the electric arc furnace in steel industry. Energy, 36(10): 6146-6155. https://doi.org/10.1016/J.ENERGY.2011.07.050
[24] García, L.M., Teruya, C.N., Valencia, R.P. (2016). Valuation of Aceros Arequipa. Bachelor's Thesis, Universidad del Pacífico. http://hdl.handle.net/11354/1460.
[25] Fan, C., Pan, F., Ma, S., Ge, Y., Zhu, Q. (2025). Hydrogen direct reduction: History and pathways for cost reduction. cScience, 1(1): e70003. https://doi.org/10.1002/csc3.70003
[26] SteelWatch. (2025). SteelWatch Explainer: Why smart use of green hydrogen is critical for steel decarbonisation. https://steelwatch.org/steelwatch-explainers/hydrogen/.
[27] Gonçalves, J.R.M., Cecílio, D.M., Oliveira, R.C.P., Mateus, M.M., Santos, D.M.F. (2022). Development of an Aspen Plus® model for the process of hydrogen production by black liquor electrolysis. Symmetry, 14(8): 1676. https://doi.org/10.3390/sym14081676
[28] Wang, J., Yang, J., Feng, Y., et al. (2025). Comparative experimental study of alkaline and proton exchange membrane water electrolysis for green hydrogen production. Applied Energy, 379: 124936. https://doi.org/10.1016/J.APENERGY.2024.124936
[29] Wang, T., Cao, X., Jiao, L. (2022). PEM water electrolysis for hydrogen production: fundamentals, advances, and prospects. Carbon Neutrality, 1(1): 21. https://doi.org/10.1007/s43979-022-00022-8
[30] Skordoulias, N., Koytsoumpa, E.I., Karellas, S. (2022). Techno-economic evaluation of medium scale power to hydrogen to combined heat and power generation systems. International Journal of Hydrogen Energy, 47(63): 26871-26890. https://doi.org/10.1016/J.IJHYDENE.2022.06.057
[31] Kumar, S., Somanna, V., Thakur, J., Gunasekara, S.N.

(2025). Exploring excess heat recovery in proton exchange membrane electrolysis for Green Hydrogen production: A Technical and economic analysis. Energy Conversion and Management, 342: 120118. https://doi.org/10.1016/J.ENCONMAN.2025.120118
[32] Hernández-Gómez, Á., Ramirez, V., Guilbert, D. (2020). Investigation of PEM electrolyzer modeling: Electrical domain, efficiency, and specific energy consumption. International Journal of Hydrogen Energy, 45(29): 14625-14639. https://doi.org/10.1016/J.IJHYDENE.2020.03.195
[33] Shiva Kumar, S., Himabindu, V. (2019). Hydrogen production by PEM water electrolysis – A review. Materials Science for Energy Technologies, 2(3): 442-454. https://doi.org/10.1016/J.MSET.2019.03.002
[34] Husaini, M.A., Darmanto, P.S., Juangsa, F.B. (2025). Integration of geothermal power plant, water treatment plant, AWE, and PEM electrolyzer for green hydrogen production: A techno-economic study. Next Energy, 7: 100288. https://doi.org/10.1016/J.NXENER.2025.100288
[35] IRENA, BlueRisk. (2023). Water for hydrogen production. International Renewable Energy Agency.
[36] El Assal, H., Camara, M.B., Guilbert, D. (2025). Advances in Electrolyzer Emulators: A Comprehensive Review. Electronics, 14(23). https://doi.org/10.3390/electronics14234576
[37] Zang, G., Graham, E.J., Mallapragada, D. (2024). H_2 production through natural gas reforming and carbon capture: A techno-economic and life cycle analysis comparison. International Journal of Hydrogen Energy, 49: 1288-1303. https://doi.org/10.1016/J.IJHYDENE.2023.09.230
[38] Rojas, F.J., Cisneros, R.F., De-La-Cruz, C., Jimenez, F. (2024). Experimental Determination of a Mixture Composed of Camisea Natural Gas and CO2 Laminar Burning Velocity. Energies, 17(22): 5529. https://doi.org/10.3390/en17225529
[39] Hamid, U., Rauf, A., Ahmed, U., Sher Shah, M.S.A., Ahmad, N. (2020). Techno-economic assessment of process integration models for boosting hydrogen production potential from coal and natural gas feedstocks. Fuel, 266: 117111. https://doi.org/10.1016/J.FUEL.2020.117111
[40] Junaedi, C., Vilekar, S.A., Walsh, D., Mastanduno, R., Morgan, C., Roychoudhury, S. (2012). Development of integrated reformer systems for syngas production. International Journal of Hydrogen Energy, 37(13): 10435-10443. https://doi.org/10.1016/J.IJHYDENE.2012.01.123
[41] Tribioli, L., Cozzolino, R., Chiappini, D. (2017). Technical assessment of different operating conditions of an on-board autothermal reformer for fuel cell vehicles. Energies, 10(7): 839. https://doi.org/10.3390/en10070839
[42] Alir, A., Tuan Abdullah, T.A., Johari, A., et al. (2023). The efficiency of carbon conversion and hydrogen production from tar steam reforming of biomass using Ni-based catalysts with alkaline earth promoters. Catalysts, 13(3): 472. https://doi.org/10.3390/catal13030472
[43] Zahid, U., Khalafalla, S.S., Alibrahim, H.A., Ahmed, U., Jameel, A.G.A. (2023). Techno-economic evaluation of simultaneous methanol and hydrogen production via autothermal reforming of natural gas. Energy Conversion and Management, 296: 117681. https://doi.org/10.1016/J.ENCONMAN.2023.117681
[44] Mu, L., Wang, S., Lu, J., Li, C., Lan, Y., Liu, G., Zhang, T. (2024). Effect of hydrogen-enriched natural gas on flue gas waste heat recovery potential and condensing heat exchanger performance. Energy, 286: 129591. https://doi.org/10.1016/J.ENERGY.2023.129591
[45] Oh, H.T., Kum, J., Park, J., Vo, N.D., Kang, J.H., Lee, C.H. (2022). Pre-combustion CO_2 capture using amine-based absorption process for blue H_2 production from steam methane reformer. Energy Conversion and Management, 262: 115632. https://doi.org/10.1016/J.ENCONMAN.2022.115632
[46] Demir, C., Løge, I.A., Jørsboe, J.K., et al. (2026). Benchmarking MDEA/PZ for CO2 absorption from high CO2-content sources: Pilot study and comparison to Aspen Plus simulations. Chinese Journal of Chemical Engineering. https://doi.org/10.1016/J.CJCHE.2025.12.035
[47] Antonini, C., Pérez-Calvo, J.F., van der Spek, M., Mazzotti, M. (2021). Optimal design of an MDEA CO2 capture plant for low-carbon hydrogen production — A rigorous process optimization approach. Separation and Purification Technology, 279: 119715. https://doi.org/10.1016/J.SEPPUR.2021.119715
[48] Hauglustaine, D. (2025). The climate benefit of a greener blue hydrogen. Scientific Reports, 15(1): 33409. https://doi.org/10.1038/s41598-025-18765-6
[49] Jiao, F., O'Neill, K.T., Al Ghafri, S., Xiao, G., May, E.F., Johns, M.L. (2025). Technoeconomic and environmental analysis of bridging blue and green hydrogen production. Energy Conversion and Management, 346: 120427. https://doi.org/10.1016/J.ENCONMAN.2025.120427
[50] Olchowik, W., Bednarek, M., Dąbrowski, T., Rosiński, A. (2023). Application of the Energy Efficiency Mathematical Model to Diagnose Photovoltaic Micro-Systems. Energies, 16(18): 6746. https://doi.org/10.3390/en16186746
[51] Moncada, J., de Goeij, B., van den Ham, J., Buskens, P., Meulendijks, N., Detz, R.J. (2025). Evaluating the costs of integrated solar hydrogen systems: Exploring the effect of scale, intermittency, and energy storage. Energies, 18(22): 6069. https://doi.org/10.3390/en18226069
[52] Shahzad, S., Alrumayh, O., Almutairi, A., Altamimi, A. (2026). Green hydrogen: A review of technological innovations, economic viability, and global prospects. Renewable and Sustainable Energy Reviews, 225: 116162. https://doi.org/10.1016/J.RSER.2025.116162

NOMENCLATURE

$\dot{m}$	Mass flow rate (kg/s)
LHV	Lower Heating Value (MJ/kg)
HHV	Higher Heating Value (MJ/kg)
P_{stack}	Power required by the PEM electrolyzer stack (MW)
P_{system}	Total system power (MW)
V	Voltage (V)
ΔG	Gibbs energy change (kJ/mol)
ΔH	Enthalpy change (kJ/mol)
ΔS	Entropy change (kJ/mol·K)

T	Temperature (K) or (°C)
F	Faraday constant (C/mol)
Q	Charge (C)
M	Module number
LCOH	Levelized Cost of Hydrogen ($/kg)
CAPEX	Capital expenditure ($)
OPEX	Operational expenditure ($/year)
r	Discount rate
t	Time (years)
N	Project lifetime (years)
PPV	Power generated by photovoltaic system (W)
APV	Area of photovoltaic panels (m^2)
GPV	Solar irradiance (W/m^2)
PEM	Proton Exchange Membrane
ATR	Autothermal Reforming
WGS	Water Gas Shift
DRI	Direct Reduced Iron
EAF	Electric Arc Furnace